Three-dimensional numerical modeling of land subsidence in Shanghai, China

Shujun Ye[1] · Yue Luo[1,2] · Jichun Wu[1] · Xuexin Yan[3] ·
Hanmei Wang[3] · Xun Jiao[3] · Pietro Teatini[4]

Abstract Shanghai, in China, has experienced two periods of rapid land subsidence mainly caused by groundwater exploitation related to economic and population growth. The first period occurred during 1956–1965 and was characterized by an average land subsidence rate of 83 mm/yr, and the second period occurred during 1990–1998 with an average subsidence rate of 16 mm/yr. Owing to the establishment of monitoring networks for groundwater levels and land subsidence, a valuable dataset has been collected since the 1960s and used to develop regional land subsidence models applied to manage groundwater resources and mitigate land subsidence. The previous geomechanical modeling approaches to simulate land subsidence were based on one-dimensional (1D) vertical stress and deformation. In this study, a numerical model of land subsidence is developed to simulate explicitly coupled three-dimensional (3D) groundwater flow and 3D aquifer-system displacements in downtown Shanghai from 30 December 1979 to 30 December 1995. The model is calibrated using piezometric, geodetic-leveling, and borehole extensometer measurements made during the 16-year simulation period. The 3D model satisfactorily reproduces the measured piezometric and deformation observations. For the first time, the capability exists to provide some preliminary estimations on the horizontal displacement field associated with the well-known land subsidence in Shanghai and for which no measurements are available. The simulated horizontal displacements peak at 11 mm, i.e. less than 10 % of the simulated maximum land subsidence, and seems too small to seriously damage infrastructure such as the subways (metro lines) in the center area of Shanghai.

Keywords Geohazards · Subsidence · Numerical modeling · Groundwater recharge · China

Published in the theme issue "Land Subsidence Processes"

✉ Shujun Ye
  sjye@nju.edu.cn

1   School of Earth Sciences and Engineering, Nanjing University, Nanjing 210023, China

2   School of Water Resource & Environmental Engineering, East China Institute of Technology, Nanchang 330013, China

3   Key Laboratory of Land Subsidence Monitoring and Prevention, Ministry of Land and Resources, Shanghai Institute of Geological Survey, Shanghai 200072, China

4   Department of Civil, Environmental and Architectural Engineering, University of Padova, Padova 35121, Italy
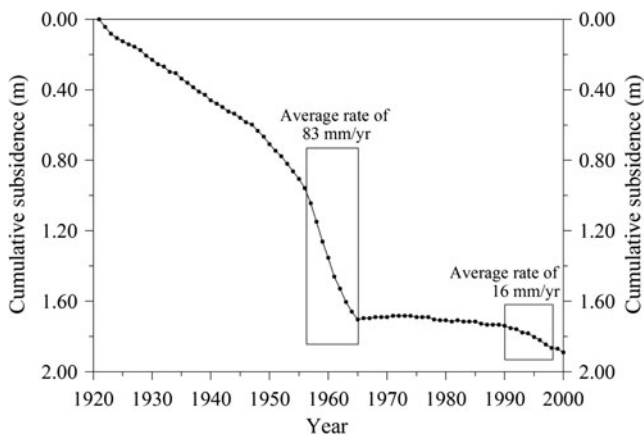
Introduction

Anthropogenic land subsidence in Shanghai, which is induced by excessive groundwater withdrawal, has been observed since the year 1921 (Zhang and Wei 2002). There have been two periods of rapid land subsidence (Fig. 1). The first occurred during 1956–1965 with an average land subsidence rate of 83 mm/yr and was associated with rapid industrialization following implementation of 'the five-year plan' in 1953. (The five-year plan is a series of social and economic development initiatives within every 5-year period, with the first plan spanning from 1953 to 1957 and the twelfth from 2011 to 2015.) The second rapid land subsidence occurred during 1990–1998 with an average land subsidence rate of 16 mm/yr and has been associated with rapid economic growth following implementation of reform and the opening-up policy measures in Shanghai since 1984. (The reform and opening-up policy was initiated in 1978 with aims to reform the economy system and open up China to the world.)

Fig. 1 Land subsidence history at Shanghai, China

The Shanghai government established extensive groundwater-level and land-subsidence monitoring networks in the mid-1980s. The first numerical model of land subsidence in Shanghai was developed in 1989 through an international collaboration project between China and Belgium (Li and Su 1991), followed by Gu et al. (1990, 1993) who developed numerical models of land subsidence in Shanghai with an emphasis on secondary consolidation effects. Because of the limited data available at that time, these earlier models were focused on the shallow sedimentary layers, i.e. the upper 100 m depth, above the second confined aquifer, and did not consider the entire aquifer system. The models simulated one-dimensional (1D) deformation. Comprehensive studies on numerical modeling of land subsidence have been conducted by researchers from Nanjing University, China, and the Shanghai Institute of Geological Survey since 2000. A regional land

subsidence model with a three-dimensional (3D) groundwater flow module and a 1D subsidence module embodying complex visco-elasto-plastic deformation characteristics with variable parameters, was developed and applied to simulate and predict land subsidence in Shanghai (Ye 2004; Ye et al. 2005, 2011; Xue et al. 2008; Shi et al. 2008; Wu et al. 2010, 2102). The 3D groundwater flow model was used to calculate the time-dependent hydraulic heads in the sedimentary sequence, and the 1D non-linear subsidence model considering delayed drainage of pore water was used to compute the time-dependent compaction of the sedimentary layers and the cumulative land subsidence.

All the land subsidence models mentioned in the preceding are based on the assumption of 1D (vertical) deformation; however, the actual deformation of the aquifer system caused by groundwater withdrawal is fully 3D (Galloway and Burbey 2011). It has been clearly demonstrated that groundwater pumping creates horizontal displacements at local and regional scales (Burbey and Helm 1999). Tensional strain resulting from horizontal displacements can generate ground ruptures/earth fissures with local damage to the surface and subsurface infrastructure (Wang et al. 2009); hence, the development of a more realistic and accurate geomechanical model, which requires determination of the 3D deformation field accompanying the 3D flow field, is needed to develop more reliable predictions of both vertical and horizontal displacements. By incorporating horizontal deformation as a component of the total volume strain, which was assumed to be represented by only vertical strain in 1D models, the total volume strain is partitioned into three components (one vertical and two horizontal strain) and

Fig. 2 Location of Shanghai City and the center area addressed in the present modeling study
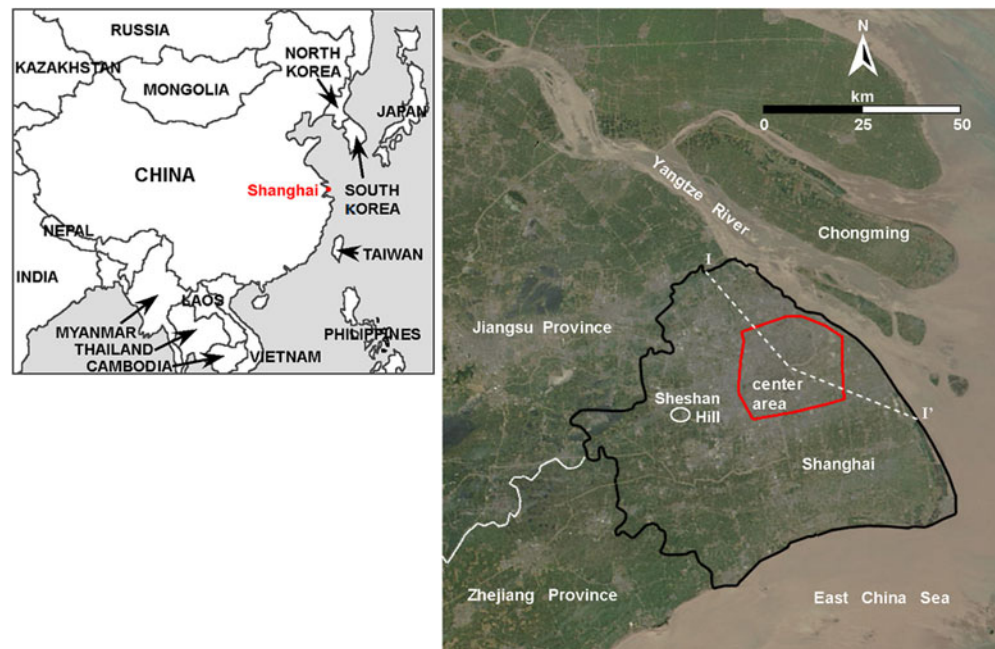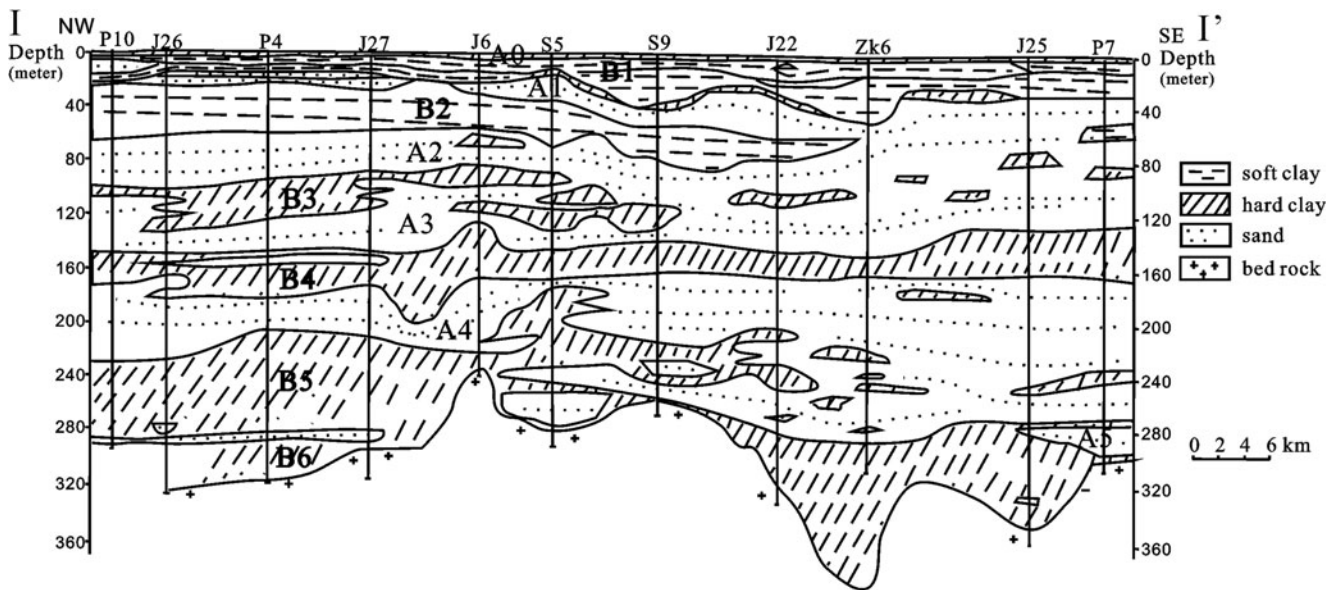
Fig. 3 Schematic stratigraphic section in Shanghai (after Ye et al. 2011). Labels *P10*, *J26*, *P4*, etc. represent the boreholes located along the section. Well/borehole correlations have been mainly used to map the various hydrostratigraphic units

therefore the corresponding (1D and 3D) aquifer-system storage coefficients are potentially different.

The deformation of an aquifer system caused by fluid withdrawal is theoretically described by the 3D fully coupled poroelasticity model originally developed by Biot (1941). Because of numerical ill-conditioning and large CPU-time constraints of coupled models when applied to regional land subsidence problems (Ferronato et al. 2001, 2012; Gambolati et al. 2011), uncoupling between the flow and the strain fields is usually assumed in hydrogeologic applications. In uncoupled formulations, which are also known as two-step (Gambolati and Freeze 1973) or explicitly coupled approaches (Teatini et al. 2011), the groundwater flow equation is first solved and then land subsidence is computed solving the equilibrium equations with the specified groundwater flow field within the porous medium. It has been demonstrated that, in anthropogenic land subsidence at the regional scale, uncoupling between the flow and the stress fields is fully

warranted on any time scale of practical interest (Gambolati et al. 2000; Teatini et al. 2006, 2010).

A 3D explicitly coupled land subsidence model is developed in this study to simulate 3D displacements caused by groundwater exploitation from the multiaquifer system in the center area of Shanghai. With an area of 660 km², downtown Shanghai is bounded by the outer ring road (red line in Fig. 2) and has experienced a cumulative land subsidence of 2 m since 1921. This zone is an important area of the city, with the densest population (10 million), a dense distribution of high-rise buildings, and crossed by 11 metro lines. Therefore, it is important to calculate the 3D deformation of the aquifer system caused by groundwater exploitation to better evaluate the possible impact on the subsurface infrastructure such as metro lines, tunnels, etc.

This paper is organized as follows. Firstly, a brief description of the deformation characteristics of sedimentary layers constituting the aquifer system in Shanghai is

Fig. 4 Time series of the annual groundwater pumping rates from the aquifer system (total, and from the *A2* and *A4* confined aquifers) of Shanghai
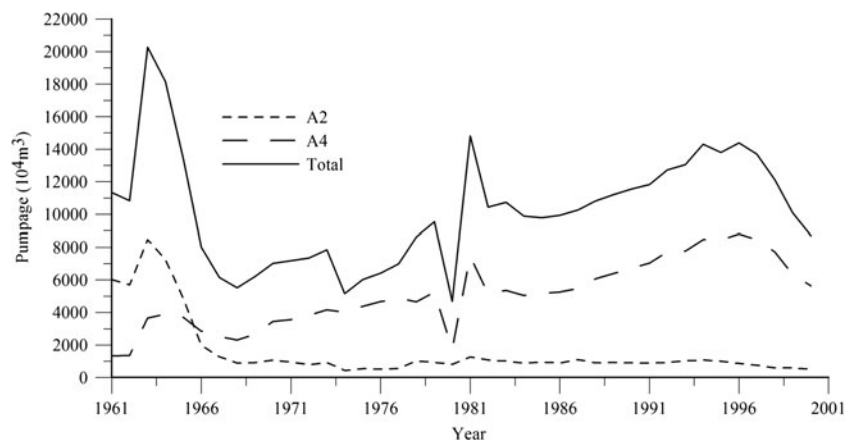
Fig. 5 Average groundwater
levels in the *A2* and *A4* confined
aquifers in Shanghai.
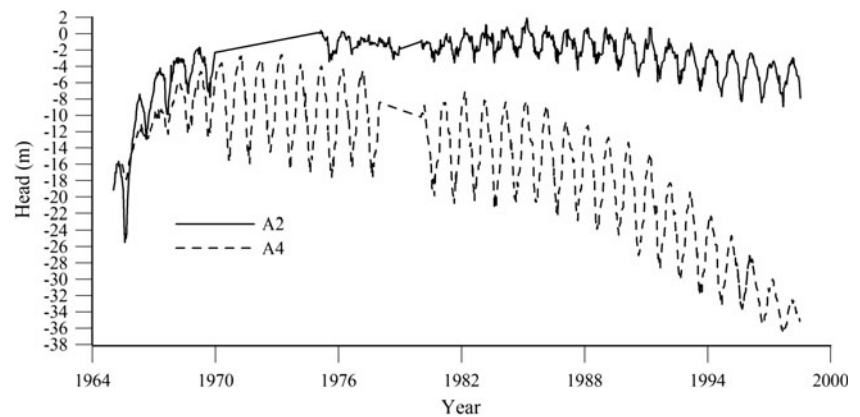
provided. Secondly, the 3D numerical model developed to
simulate 3D groundwater flow and the 3D displacement
field in the center area of Shanghai is presented. Thirdly,
the results obtained by the model for the period from
December 30, 1979 to December 30, 1995, are described
and discussed.

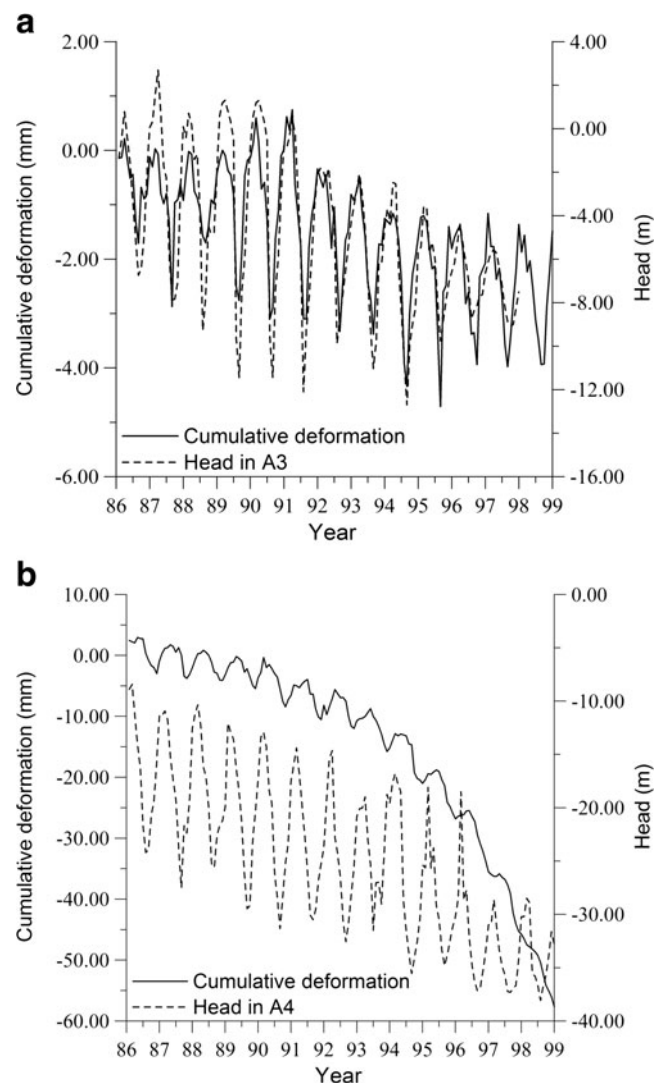## Deformation characteristics of sedimentary layers in Shanghai

Shanghai city lies in the eastern portion of the Yangtze Delta
and is composed of a mainland zone (the area bounded by the
black line in Fig. 2) and three islands in the Yangtze River,
with a cumulative land area equal to about 6,780 km^2. The
municipality is bounded by the East Sea to the east, and the
Jiangsu Province and Zhejiang Province to the west (Fig. 2).

The aquifer system is composed of Quaternary unconsoli-
dated sediments including clay, silt, sandy clay, and sand. The
sediments are generally 200–350 m thick with bedrock under-
lying the alluvial deposits except for the outcrop at Sheshan
Hill (Fig. 2). The sedimentary layers are divided into aquifers
and aquitards according to lithology. The multiaquifer system
comprises a phreatic aquifer (named A0), five confined aqui-
fers (named from A1 to A5) and six intervening aquitards
(named from B1 to B6; Fig. 3). The aquifers and aquitards
are not continuous in Shanghai.

Excessive groundwater withdrawal from the aquifer sys-
tem, especially from A2 and A4 during the 1950s and 1960s
with a maximum total withdrawal of 200 million m^3/yr in
1963, and during the mid-1980s to late 1990s with a maxi-
mum total withdrawal of 143 million m^3 in 1994 (Fig. 4), has
caused significant groundwater level declines in A2 and A4
(Fig. 5). Groundwater-level declines result in effective stress
increases and compaction to different extents of the various
sedimentary layers (Fig. 6).

The deformation characteristics of the sedimentary layers
vary because of differences in lithology, thickness, applied
stress, and stress history, which has been accurately described

in the literature (Xue et al. 2008; Ye et al. 2011, 2012). A short
summary of the most important information is provided here.
The A0, A1, A2, A3, A5, B3, B5 and B6 aquifers and

Fig. 6 Cumulative deformation vs. hydraulic head **a** in aquifer A3 at
extensometer F10-5 and **b** in aquifer A4 at extensometer F10-2. The
location of extensometer F10 is provided in Fig. 9

aquitards have mainly elastic deformation characteristics (Fig. 6a) with small compressibility values. Deformations of B1 and B2 are mainly plastic with a little elastic component and some creep (Ye et al. 2011). B4 and A4 have similar deformation features (Ye et al. 2011), that is the deformation is mainly elastic where the groundwater level declines were small, but mainly plastic in places where the groundwater levels changed significantly during the 1990s (Fig. 6b).

Model setup

Explicitly coupled 3D land subsidence model

In geomechanical investigations of land subsidence accompanying 3D aquifer-system deformation at regional scales, a two-step or explicitly coupled approach typically is used to solve the uncoupled groundwater flow and deformation equations for fluid pore pressures (equivalent hydraulic heads) and displacements at any time scale of practical interest (Gambolati et al. 2000; Teatini et al. 2006, 2010). In this study, such an explicitly coupled approach is followed, with the flow field initially computed at each time step and the deformation then calculated based on the known pore pressure gradients.

The 3D uncoupled land subsidence model is expressed as (Verruijt 1969):

$$\frac{E}{2(1+\nu)}\left(\frac{1}{1-2\nu}\frac{\partial\varepsilon}{\partial x} + \nabla^2 u_x\right) = \frac{\partial P}{\partial x} \tag{1}$$

$$\frac{E}{2(1+\nu)}\left(\frac{1}{1-2\nu}\frac{\partial\varepsilon}{\partial y} + \nabla^2 u_y\right) = \frac{\partial P}{\partial y} \tag{2}$$

$$\frac{E}{2(1+\nu)}\left(\frac{1}{1-2\nu}\frac{\partial\varepsilon}{\partial z} + \nabla^2 u_z\right) = \frac{\partial P}{\partial z} \tag{3}$$

$$\frac{\partial}{\partial x_i}\left(K_{ij}\frac{\partial H}{\partial x_j}\right) = S_s\frac{\partial H}{\partial t} + q \quad i,j = x,y,z \tag{4}$$

where E is the Young modulus, ν is the Poisson ratio, u_x, u_y and u_z are the displacement components along the coordinate axes x, y and z, respectively, ε is the volume strain $\varepsilon = \frac{\partial u_x}{\partial x} + \frac{\partial u_y}{\partial y} + \frac{\partial u_z}{\partial z}$, P is the pore water pressure, which is equal to $\gamma_w \cdot H$ with γ_w the specific weight of water and H the hydraulic head, and ∇^2 is the Laplace operator. In Eq. (4), $K_{i,j}$ is the hydraulic conductivity tensor, t is time, q is the source/sink term, and S_s is the specific storage $S_s = \gamma_w(\alpha + n\beta)$, with α the matrix compressibility, which is related to the Young modulus and Poisson ratio through $\alpha = \frac{(1+\nu)(1-2\nu)}{E(1-\nu)}$, n is the medium porosity, and β the water volumetric compressibility. The parameter α is nonlinear and takes the elastic value

Fig. 7 Comparison between the displacement components on the aquifer top as calculated by the explicitly coupled 3D model developed in this study and COMSOL for the simple test case used to verify the model accuracy. a Vertical displacement, b horizontal displacement
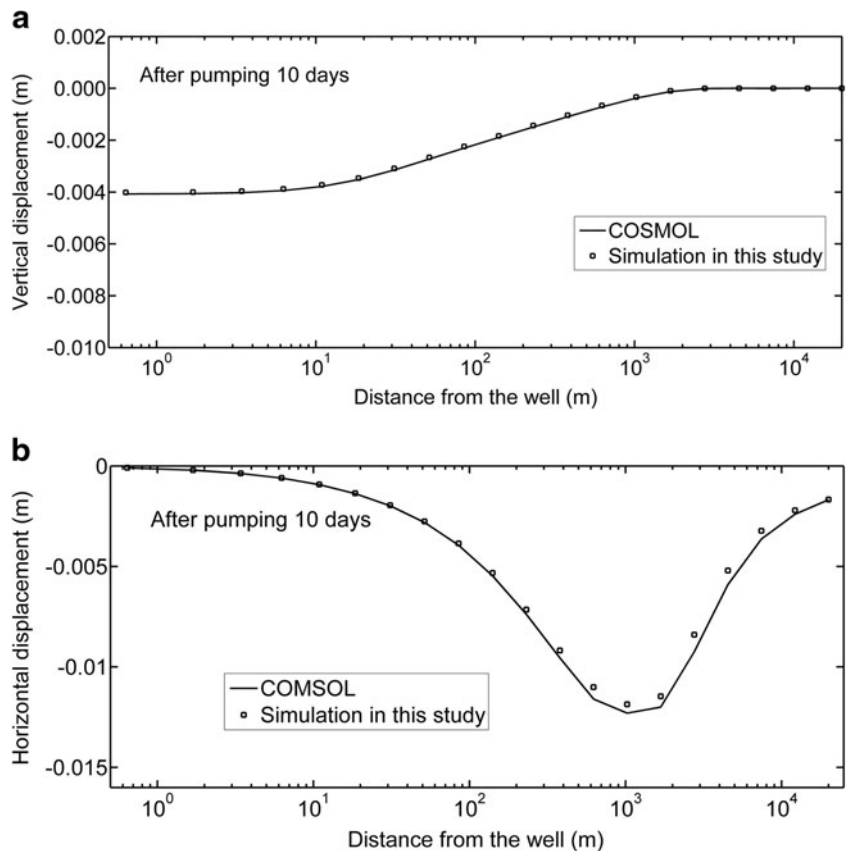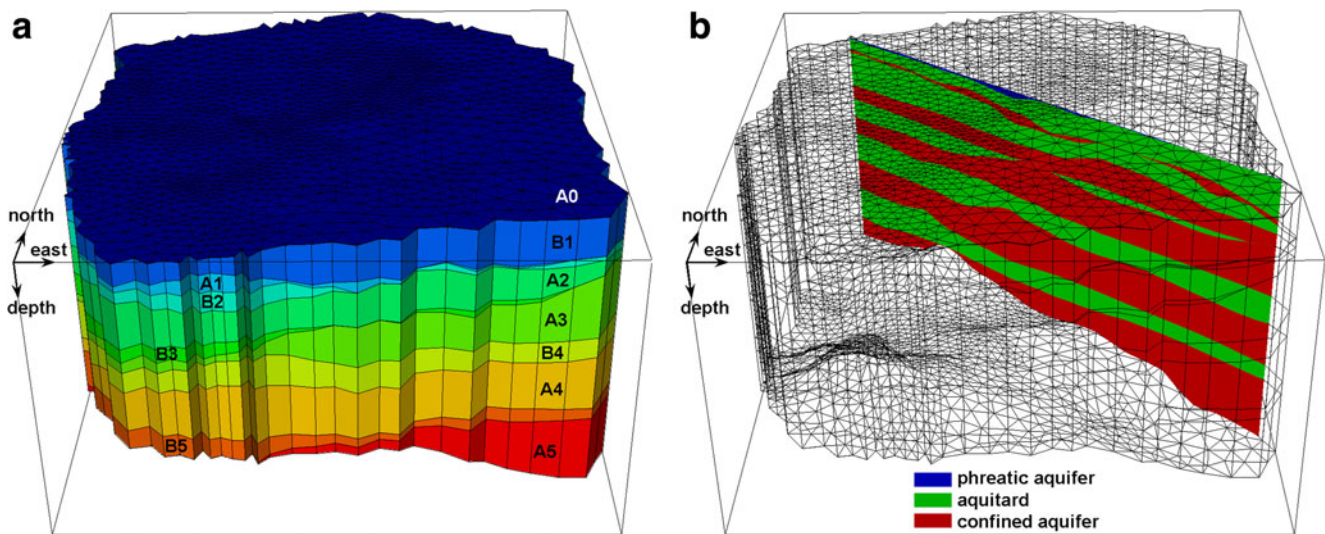
Fig. 8 Perspective views of the 3D finite-element mesh of the center area of Shanghai. The various geologic layers are distinguished (**a**). **b** The hydro-stratigraphic units are *highlighted* on the *center part* of the vertical section passing along the *I–I'* profile traced in Fig. 2

α_{ke} when the effective stress is less than the preconsolidation stress, otherwise α takes the plastic value α_{kv} (Ye et al. 2011, 2012). The specific storage is denoted by S_{se} and S_{sv}, accordingly. Special care must be taken in the explicitly coupled approach to use S_s values in the groundwater flow Eq. (4) that are consistent with those used for the geomechanical parameters E and ν in the equilibrium Eqs. (1)–(3). The S_s as defined in the classic theory of transient groundwater flow assumes 1D vertical stress and strain (Freeze and Cherry 1979).

Numerical scheme and model verification

The standard finite element (FE) Galerkin method is used to solve the explicitly coupled 3D land subsidence model. Triangular prisms are used for the space discretization and a weighted finite difference approach is implemented for time stepping in the flow model. The groundwater flow field is computed first at each time step, and displacements are then calculated using the pore pressure gradient as a known source of strength in the geomechanical model. The flow model is strictly consistent with the geomechanical model in the sense that the same 3D grid is used, with the storage coefficient variable in time and space as it is expressed in terms of E in the geomechanical model. At the end of each time step, the need for updating the oedometric compressibility with respect to its elastic or plastic value, and consequently the specific storage and Young modulus, is checked in each element by comparing the simulated value of the hydraulic head (and hence the corresponding effective stress) with the lowest hydraulic head, known from the observations and the modelling outcome (the corresponding preconsolidation stress). A conjugate gradient-like iterative algorithm with an advanced block FSAI-ILU (Factored Sparse Approximate Inverse with

Incomplete LU factorization) preconditioner (Janna et al. 2010) are implemented in the models to effectively solve the large linear systems arising from the FE implementation.

The model has been validated against existing codes, in particular COMSOL (COMSOL 2014). A simplified test case is presented here to provide verification of the model correctness. The modeling domain is rectilinear with a single 30-m-thick confined aquifer with an areal extent of 40×40 km. Groundwater is withdrawn at a constant pumping rate equal to 1,000 m³/day from a well located in the middle of the
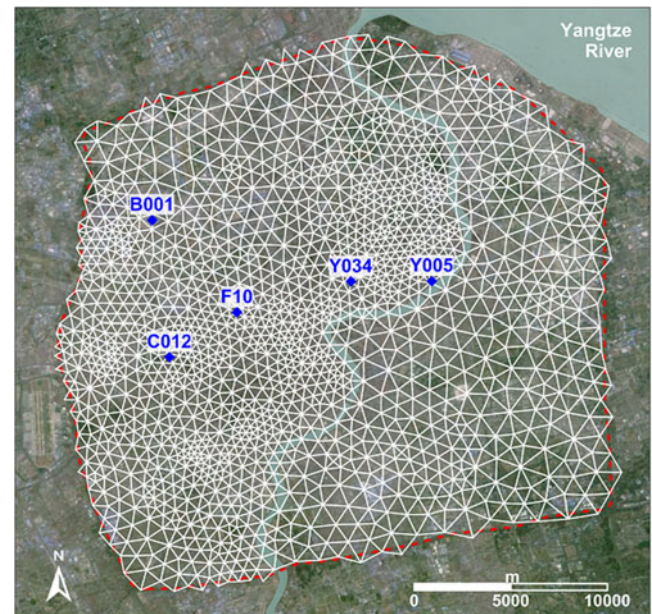
Fig. 9 Horizontal projection of the 3D mesh, corresponding to the triangular grid used to discretize the surface of each aquifer or aquitard. The location of the monitoring wells and the F10 extensometer, whose records are plotted in Figs. 13 and 16, respectively, are provided
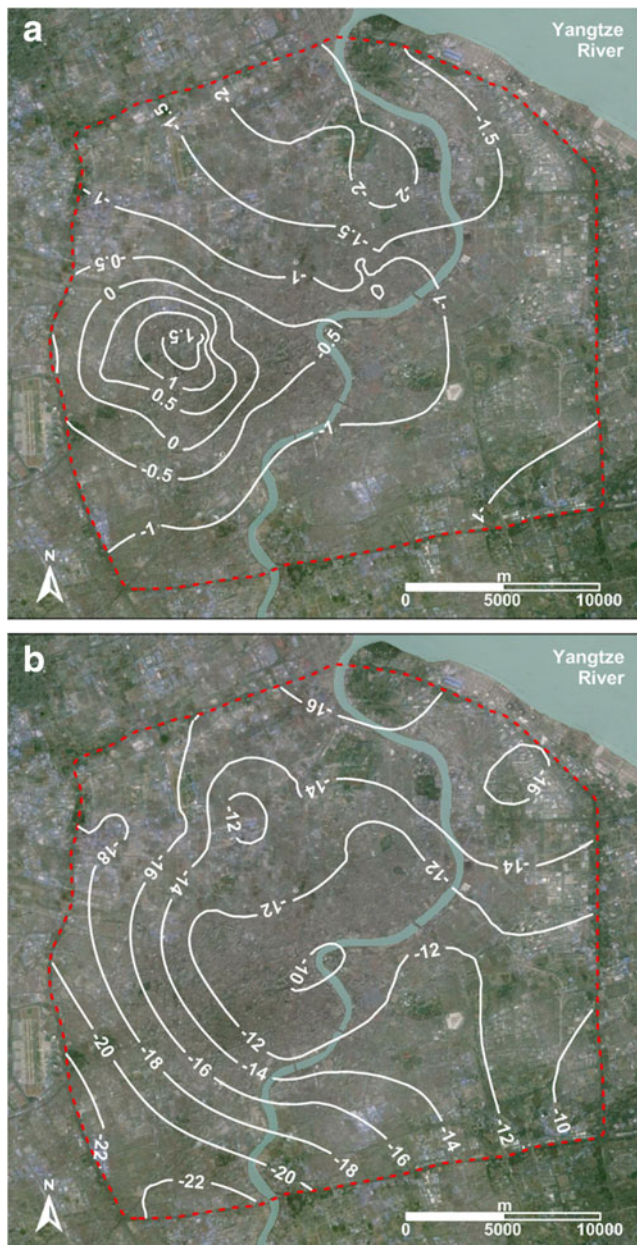
Fig. 10 Discharge and recharge wells in aquifers **a** A2 and **b** A4. *White-to-red triangles* represent the discharge wells (negative values), *white-to-blue circles* represent the recharge wells (positive values). The *symbol size* is proportional to the average yearly rate over the 16-year simulation period
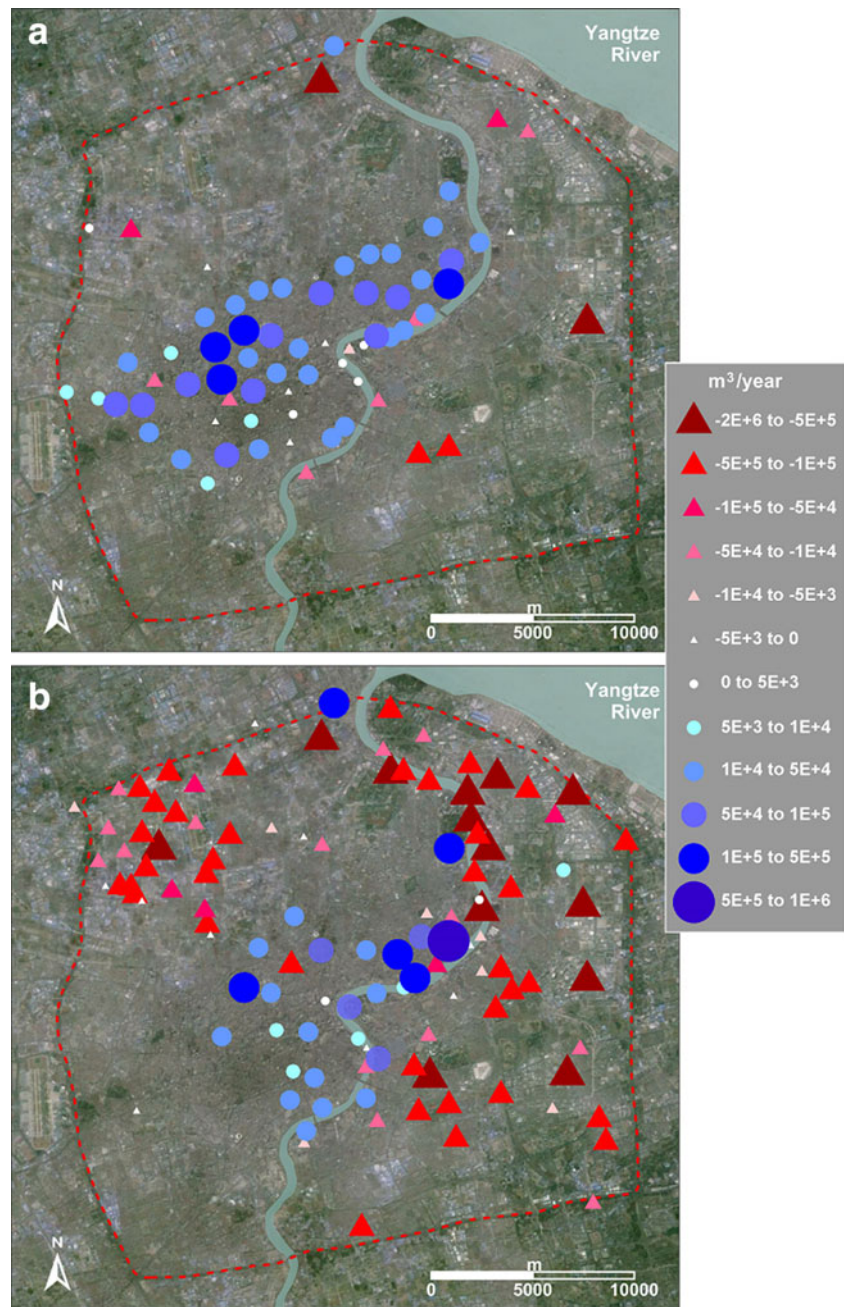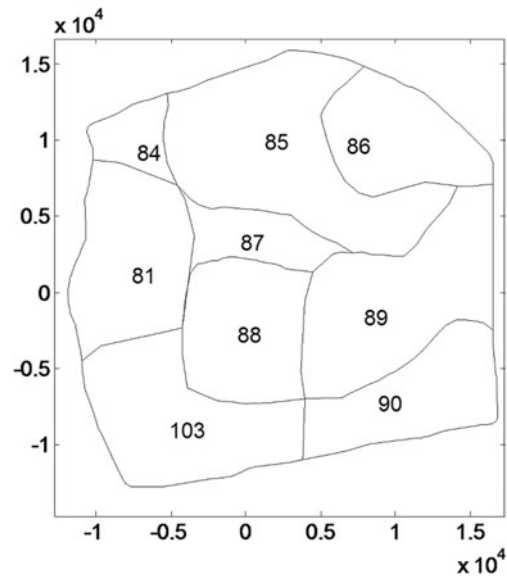

aquifer. The aquifer is homogeneous with $K = 10$ m/day, $E = 10^7$ kg/m^2, and $\nu = 0.3$. Initial heads are 0 m. Boundary conditions of the flow model include impermeable top and bottom boundaries and a 0-m fixed head on the lateral boundaries. A standard Dirichlet condition with fixed bottom boundary is assumed in the geomechanical model. The study area is discretized into 1,600 triangular prisms, with a finer grid close to the well. Comparison of simulated results from the explicitly coupled model and COMSOL is shown in Fig. 7, which presents the vertical and horizontal displacements of the top surface after a pumping period of 10 days. The two codes provide almost identical results.

Numerical simulation of 3D land subsidence in Shanghai

The simulated domain, which is the center area of Shanghai (Fig. 2), comprises the material between ground surface and a rigid 250–300 m deep basement. The domain is spatially discretized using a 3D mesh consisting of 19,524 nodes and 34,309 triangular prisms to accurately represent the multiaquifer system including six aquifers and five aquitards (Fig. 8). There are 11 layers representing the 6 aquifers and 5 aquitards, and 12 surfaces with 1,627 nodes and 3,119 triangles for each surface which represent the tops and bottoms of each aquifer and aquitard (Fig. 9). The element size in the horizontal

Fig. 12 Model parameter subzones in aquitard B5. Axis units are m in the Shanghai local coordinate system

plane ranges from 0.017 to 0.624 km². Zero flux on the basement boundary and Dirichlet conditions on the top and lateral boundaries are prescribed in the flow model. The prescribed hydraulic heads on the top and lateral boundaries were obtained from the larger-extent groundwater flow model developed for Shanghai city to simulate the period 1961–2005 (Xue et al. 2008). A Dirichlet condition with fixed bottom boundary and a traction-free surface are assumed in the geomechanical model. Two different boundary conditions are tested on the lateral boundaries in the geomechanical model. In the first case, a Dirichlet condition with fixed boundary is prescribed, and in the other a traction-free lateral boundary is used.

The simulations span the interval from December 30, 1979 to December 30, 1995, which is a period characterized by a significant increase in groundwater pumping and corresponding large groundwater-level declines in A4 (Fig. 5). Figure 10 shows the discharge and recharge wells with the average annual discharge and recharge rates in A2 and A4. There are many recharge wells and a few discharge wells in A2, and many discharge wells with high flow rates and some recharge wells with low flow rates in A4. The 16-year long simulation period is divided into 64 tri-monthly time steps. The initial

Fig. 11 Initial (30 December 1979) potentiometric surfaces (head in m above msl) in aquifers **a** A2 and **b** A4

Table 1 Hydro-geomechanical parameters used in the final simulation of the 3D groundwater flow and geomechanical models

Aquifer/aquitard	K_{xx} (m/day)	K_{yy} (m/day)	K_{zz} (m/day)	S_{se} (1/m)	S_{sv} (1/m)
A1	1–10	1–10	0.1–1	10^{-6}–10^{-5}	10^{-6}–10^{-5}
A2	2–50	2–50	0.2–5	10^{-6}–10^{-5}	10^{-6}–10^{-5}
A3	7–30	7–30	0.7–3	10^{-6}–10^{-5}	10^{-6}–10^{-5}
A4	1–40	1–40	0.1–4	10^{-6}–10^{-5}	10^{-6}–10^{-4}
A5	1–20	1–20	0.1–2	10^{-6}–10^{-5}	10^{-6}–10^{-5}
B1–B5	10^{-2}–10^{-5}	10^{-2}–10^{-5}	10^{-3}–10^{-6}	5×10^{-6}–5×10^{-5}	9×10^{-6}–8×10^{-4}

Table 2 Summary of the hydraulic conductivity and geomechanical parameters used in the nine subzones into which aquitard B5 is subdivided

Subzone No.	K_{xx} (m/day)	K_{yy} (m/day)	K_{zz} (m/day)	S_{se} (m^{-1})	S_{sv} (m^{-1})
81	2.50×10^{-5}	2.50×10^{-5}	2.50×10^{-6}	7.50×10^{-6}	1.50×10^{-5}
84	2.08×10^{-3}	2.08×10^{-3}	2.08×10^{-4}	7.58×10^{-6}	1.52×10^{-5}
85	2.50×10^{-3}	2.50×10^{-3}	2.50×10^{-4}	7.43×10^{-6}	1.49×10^{-5}
86	4.00×10^{-2}	4.00×10^{-2}	4.00×10^{-3}	7.43×10^{-5}	1.49×10^{-4}
87	2.50×10^{-3}	2.50×10^{-3}	2.50×10^{-4}	8.02×10^{-6}	1.60×10^{-5}
88	2.50×10^{-3}	2.50×10^{-3}	2.50×10^{-4}	7.50×10^{-6}	1.50×10^{-5}
89	6.00×10^{-3}	6.00×10^{-3}	6.00×10^{-4}	8.10×10^{-6}	1.62×10^{-5}
90	4.00×10^{-3}	4.00×10^{-3}	4.00×10^{-4}	7.95×10^{-6}	1.59×10^{-5}
103	3.13×10^{-8}	3.13×10^{-8}	3.13×10^{-9}	7.43×10^{-7}	1.49×10^{-6}

groundwater levels in A2 and A4 are shown in Fig. 11. In A2 the groundwater levels ranged from −1.5 to 2 m above mean sea level (msl) and groundwater generally flowed from west to east. The groundwater levels ranged from −22 to −10 m above msl in A4 and groundwater generally flowed from east to west.

Modeling results and discussion

Parameter subzones and parameter values

The aquifer system was divided into 103 subzones according to the differences in lithologic, hydraulic, and mechanical properties of sediments. Due to a lack of specific information, Poisson's ratio ν was set to 0.3, which is a typical values for recent sedimentary deposits (Comerlati et al. 2004; Teatini et al. 2006). The calibration of parameters was carried out by a trial and error procedure. The calibrated values of

hydraulic conductivity, elastic and plastic specific storage of aquifers and aquitards are provided in Table 1. Taking B5 as an example, the model layer is divided into nine subzones (Fig. 12). The calibrated parameter values for each subzone are shown in Table 2.

Comparing the calibrated parameters of the previous 1D land subsidence models (Ye et al. 2011; Luo et al. 2016) with those obtained in the present 3D model, shows that matrix compressibility is relatively smaller (20 %) in the 3D model with respect to the 1D model, and aquitard hydraulic conductivity in the vertical direction is higher in the 3D model with K_{zz} of 10^{-6}–10^{-3} m/day than that in the 1D model with K_v of 10^{-8}–10^{-5} m/day (Luo et al. 2016). This would indicate that generally there would be less delay in compaction of aquitards in the 3D model as compared with the 1D model, and for equivalent minimum heads in the aquitards there would be more ultimate compaction in the 1D model compared with the 3D model.

Fig. 13 Calculated versus measured groundwater levels in the four boreholes whose locations are provided in Fig. 9
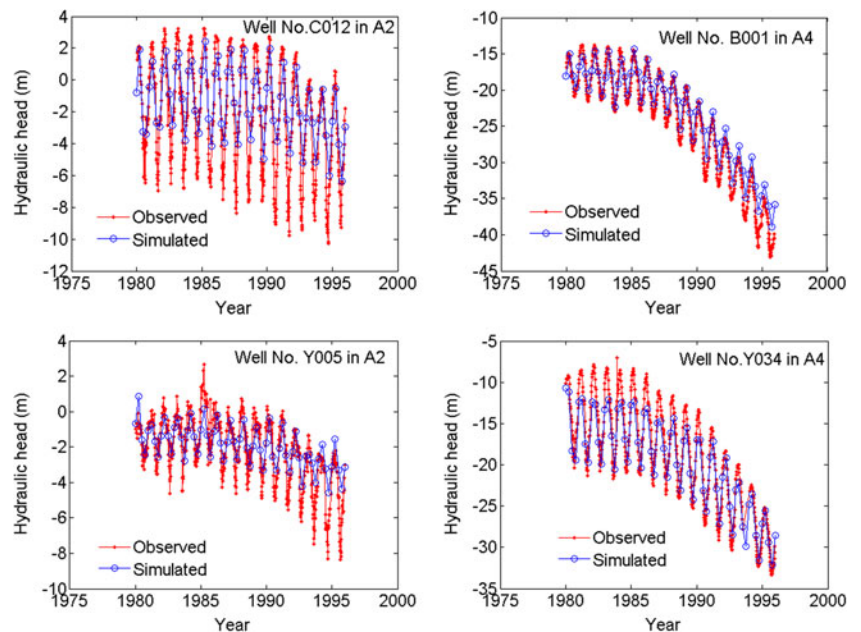
Groundwater levels

Figure 13 compares the model results and the measured head in a few observation wells whose locations are shown in Fig. 9. The simulated heads agree generally well with the observed heads. The long-term and seasonal trends are satisfactorily captured; the seasonal peak values (both minima and maxima) are underestimated and this is attributed to the tri-monthly simulation time step which is much larger than the groundwater-level measurement interval.

Figures 14 and 15 show the piezometric-surface maps for A2 and A4 on December 30, 1995, respectively. In both aquifers, the simulated piezometric surfaces (Figs. 14a and 15a) agree well with those derived by interpolating the observed heads (Figs. 14b and 15b). The simulated heads range from −6 to −3 and −38 to −22 m above msl in aquifers A2 and A4, respectively, with declines of about 2–4 and 10–20 m in A2 and A4, respectively compared to the initial heads on December 30, 1979. The inferred groundwater flow patterns in A2, from 1979 to 1995, shift from predominantly away from a groundwater mount (in the west) in all directions to predominantly toward a drawdown cone (in the west) in all directions, and in A4 shift from predominantly away from the
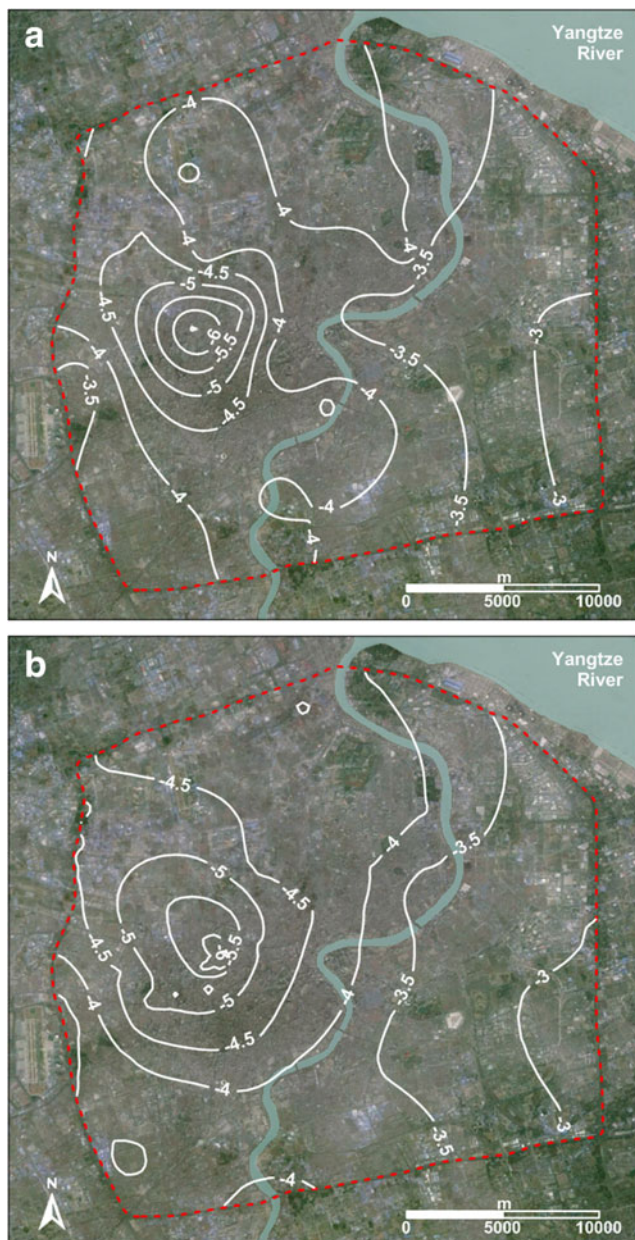
Fig. 14 a Simulated and **b** measured piezometric surfaces (head in m above msl) in aquifer A2 on 30 December 1995, at the end of the simulation period
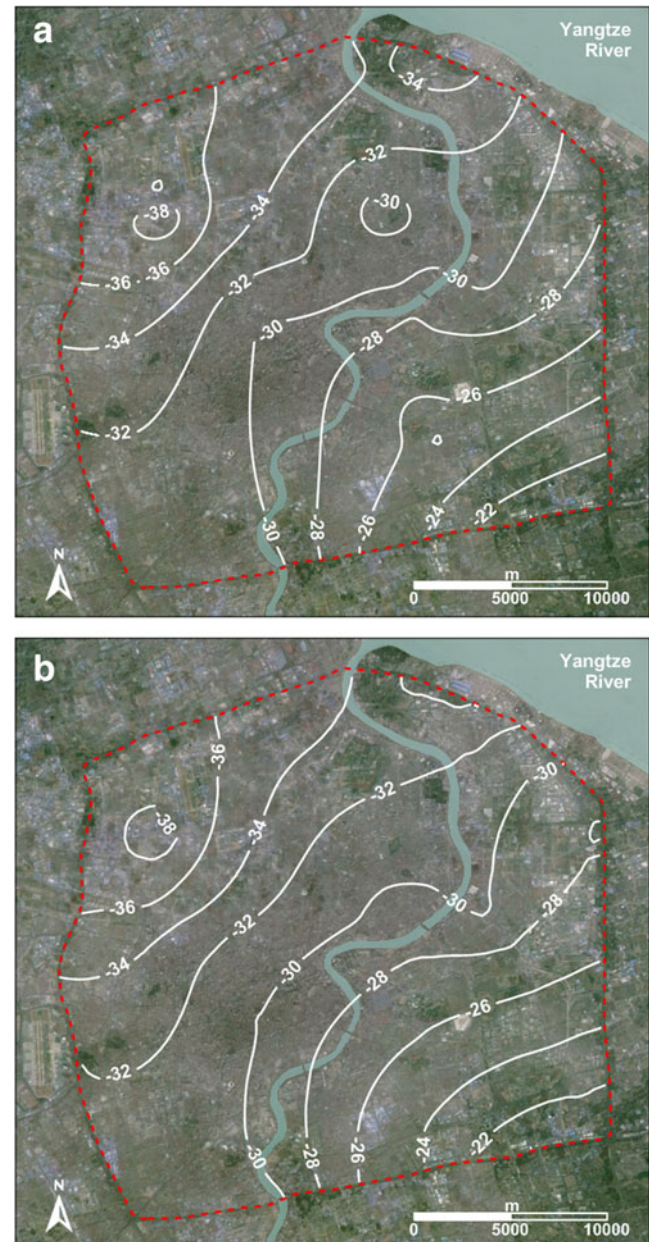
Fig. 15 a Simulated and **b** measured piezometric surfaces (head in m above msl) in aquifer A4 on 30 December 1995, at the end of the simulation period

city center in all directions with the strongest gradient toward the southwest to predominantly southeast to northwest through the city center.

Deformation and land displacements

Figure 16 compares the model results in terms of vertical compaction/expansion and the observed deformation in a few depth intervals monitored at the F10 extensometric station. Both the computed long-term compaction as well as the seasonal compaction/expansion are in good agreement with the observed values. As expected from the model outcome in terms of piezometric evolution (Fig. 13), the relatively large time step used in the simulations results in underestimated

seasonal deformation peaks. It should be noted that prior to the beginning of the simulation period, the aquitards would already be in a state of disequilibrium with respect to historic drawdowns in the adjacent aquifers, and releasing groundwater to the aquifers and compacting at the start of the simulation. Owing to a lack of information on heads and compaction in the aquitards, the disequilibrium conditions in the aquitards were ignored, which could result in less simulated deformation.

The cumulative land subsidence computed and measured over the 16-year simulation period is shown in Fig. 17. Figure 17a highlights simulated vertical displacements (land subsidence) as much as 0.25 m, with a range between 0.10 and 0.25 m in the Shanghai downtown area. Land subsidence

Fig. 16 Simulated and measured vertical deformation (negative values denote compaction) for some depth intervals at the F10 extensometer. Sediments at depths of **a** 165–294 m, **b** 124–165 m, **c** 78–124 m, **d** 26–78 m , and **e** 1–26 m
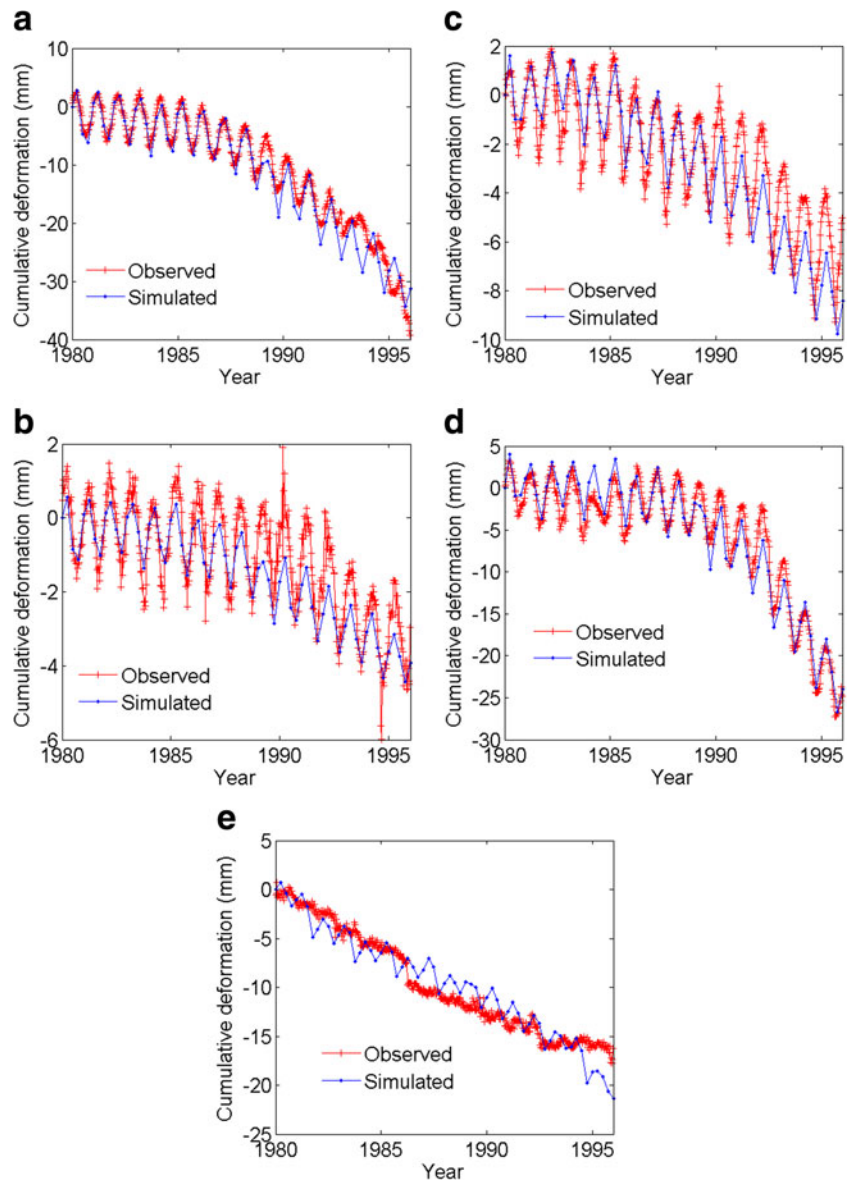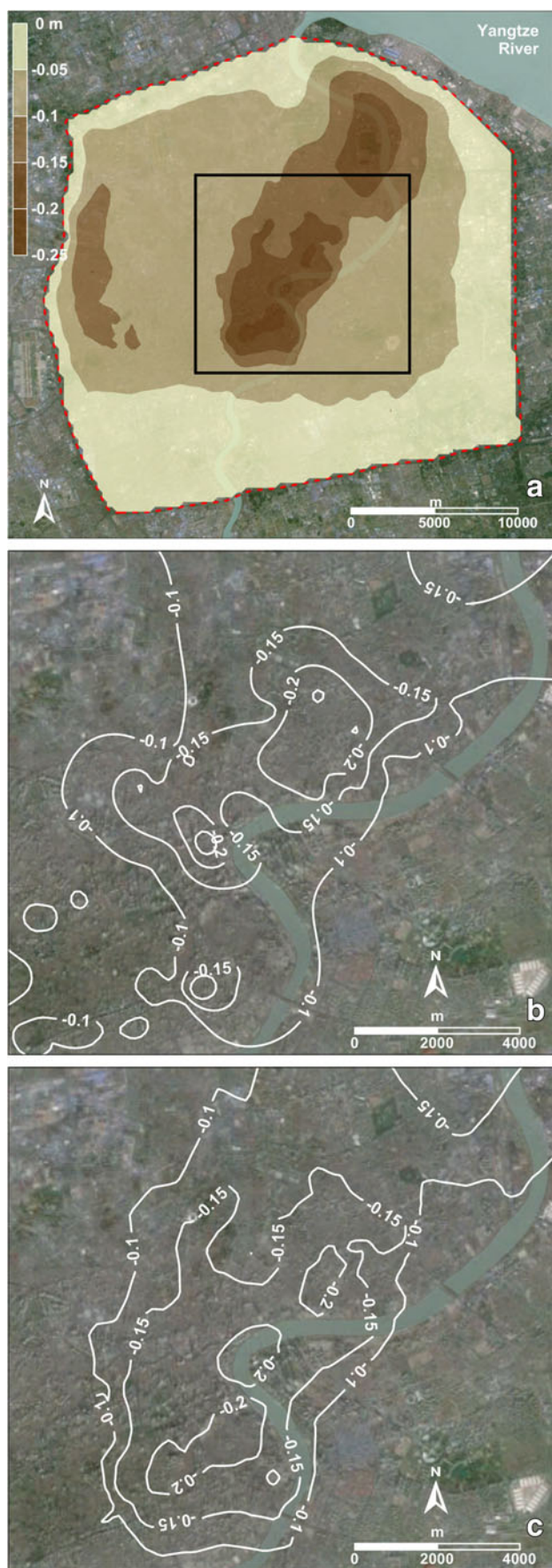
◀ **Fig. 17** **a** Cumulative land subsidence (in m) at Shanghai obtained by the 3D geomechanical model. Simulated (**b**) and measured (**c**) cumulative land subsidence on 30 December 1995, in the downtown area (*black square* in **a**)

vanished at the boundary of the study area due to the boundary condition implemented. A specific discussion on this issue is provided in the next section. Long time records of land subsidence measured by leveling are available in the downtown area from Dec. 30, 1979 to Dec. 30, 1995. Figure 17b,c shows that the simulated and measured cumulative land subsidence in the downtown area over the 16 years of simulation satisfactorily agree.

Figure 18 shows the vector maps of the cumulative horizontal displacement at the bottom of the A2 and A4 confined aquifers. The maximum values are calculated in the range between 0.004 and 0.008 m. The magnitude of the horizontal displacements is mainly related to the local compressibility and change in groundwater level. The higher values usually correspond to the larger compressibility and groundwater level decline. Taking Fig. 18b as an example, where the horizontal displacement vectors at the interface between A4 and B5 are shown, the largest horizontal displacements are obtained in the north-eastern part of the map, which corresponds to the zone with the largest changes in groundwater levels caused by the significant pumping rate in some wells (Fig. 10b) and also the highest compressibility in subzone No. 86 (Fig. 12 and Table 2). In the northeast area where the horizontal vectors are largest, they seem to be pointing away from a region centered on the river. If there is a single well pumping, the horizontal deformation will extend well beyond the drawdown and the maximum horizontal deformateon is not correlated with the maximum head decline because the maximum deformation migrates outward from the pumping well as the square root of time (Helm 1994). From Fig. 10b, one can see most of the pumping wells are on either side of the river. So the pattern of pointing away from a region centered on the river with the largest horizontal vectors could have resulted from the mixed effects of many pumping wells, distances from wells and pumping time.

It is worth noting that the cumulative horizontal displacements are all less than 0.008 m except at the ground surface where a maximum 0.011 m horizontal displacement is computed. Unfortunately, no observations of horizontal displacements are available to date. Currently, no earth fissure associated with anthropogenic land subsidence has been observed in Shanghai.

Finally, it is worth comparing the results presented in the preceding with the outcomes obtained by the previous 1D models (e.g., Ye et al. 2011). Although the simulated time intervals differ somewhat, the two modelling approaches have provided similar results in terms of vertical land
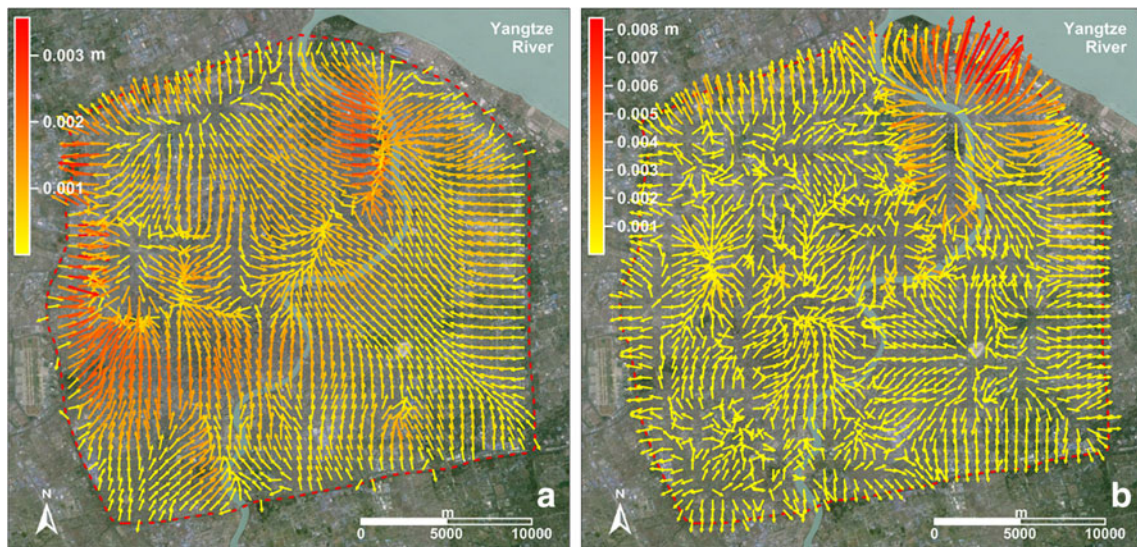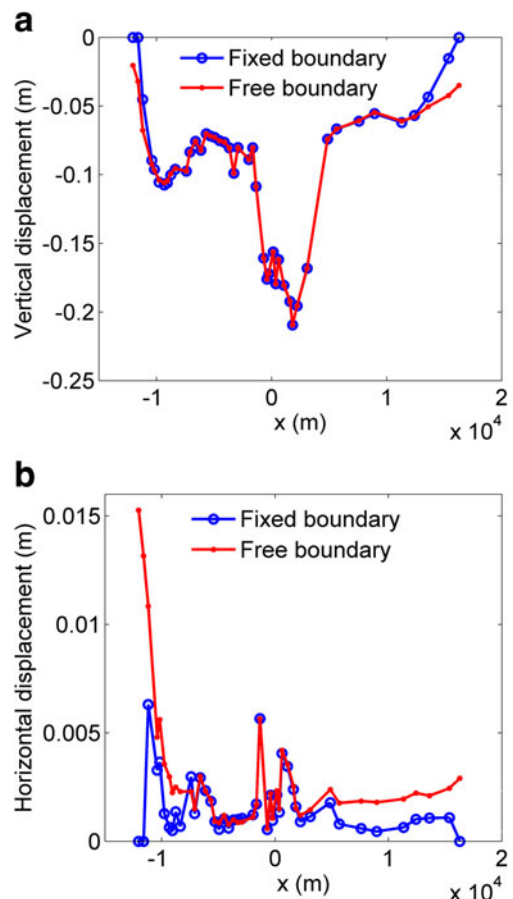
Fig. 18 Simulated cumulative horizontal displacements (for the period 30 December 1979 to 30 December 1995) in aquifers **a** A2 and **b** A4

displacements. Moreover, the horizontal displacements provided by the 3D model are quite small as already discussed, which seems to suggest that the three-dimensionality of the deformation is negligible at this scale (municipality) of investigation, possibly due to the relatively shallow depth of the compacting/expanding units and the scattered distribution of the pumping/recharging wells, whose effects in terms of horizontal displacements cancel or at least reduce each other. Also the relative coarse grid used to discretize the multiaquifer system has surely contributed to smoothing, and hence reducing, the computed maximum horizontal displacements. However, the effort required from using a much refined grid resolution (on the order of one million nodes) will be valuable only when detailed measurements of the horizontal movements are available to calibrate the model.

Impacts of boundary conditions of 3D geomechanical model

As reported in the preceding, two different lateral boundary conditions were tested in the 3D geomechanical model. One was a fixed boundary, and the other was a traction-free boundary. Figure 19 shows the simulated vertical and horizontal displacements as obtained implementing the two lateral boundary conditions along a west–east profile whose starting and end points are on the lateral boundary and which passes through the center of the study area. The vertical and horizontal displacements simulated using a Dirichlet condition with fixed boundary are 0 m on the boundary, but those simulated using a traction-free boundary are obvious and non zero, ranging from about 0.002 to 0.004, and 0.003 to 0.015 m on the boundary for vertical and horizontal displacements, respectively. The differences between the results are significant only in a relatively narrow strip along the domain boundary, with

the two outcomes superposing in the downtown area. Notice that the horizontal displacements are influenced by the boundary conditions more than the vertical displacements (Fig. 19).

Fig. 19 Comparison between the simulated **a** vertical and **b** horizontal displacements provided by the geomechanical model using two alternative boundary conditions (fixed, and traction-free) along a west–east profile through the Shanghai downtown area

Summary and conclusions

A 3D explicitly coupled geomechanical model is developed to simulate the groundwater level changes and 3D displacements in the aquifer system underlying the center area of Shanghai due to groundwater withdrawal and recharge between December 30, 1979, and December 30, 1995. Elastic and plastic compressibility values are appropriately considered in the groundwater flow and geomechanical models depending on the actual effective stress with respect to the preconsolidation stress.

The simulation results satisfactorily agree with the available observations of head, vertical displacement in the aquifer system, and land subsidence. The groundwater levels declined 2–4 and 10–20 m in the second (A2) and fourth (A4) confined aquifers, respectively, due to the significant increase in groundwater pumping from these two major aquifers during the simulation period. As much as 250 mm of cumulative land subsidence occurs in the downtown area and the cumulative horizontal displacement peaks 11 mm on the ground surface and is smaller than 8.5 mm at depth.

Alternative fixed and traction-free boundary conditions imposed on the lateral boundary of the geomechanical model, show limited differences in deformation in a relatively narrow strip close to the model boundary. The horizontal displacements appear more influenced by the boundary conditions than is land subsidence. The model is limited by the lack of horizontal displacement measurements for model calibration and verification. It can be concluded that the 3D explicitly coupled geomechanical model can simulate the 3D displacement field of the aquifer system in the center area of Shanghai.

This is the first 3D land subsidence model developed for Shanghai. The simulated land subsidence (vertical displacement) and horizontal displacements can be used to evaluate the impact of the groundwater management, such as the effects of groundwater pumpage on surface and subsurface infrastructure (for example the many metro lines and tunnels, etc. crossing the central area of Shanghai). The results of this study highlight that the horizontal displacements caused by regional groundwater exploitation seem too small to severely damage the subsurface infrastructure in the center area of Shanghai; however, more local (site-specific) investigations are needed.

This 3D geomechanical model must be considered as a first attempt that could be notably improved in the future by considering more accurate constitutive relationships of the geomechanical parameters, a finer grid in the horizontal plane where the largest horizontal displacements have been calculated and in the vertical dimension in some thick aquifers and aquitards, and more appropriate boundary conditions derived from regional land subsidence models addressing the entire Yangtze River delta. Moreover, a more precise calibration at the local scale will be done in a further study by using the horizontal and vertical displacements obtained by InSAR.

References

Biot MA (1941) General theory of three-dimensional consolidation. J Appl Phys 12(2):155–164

Burbey TJ, Helm DC (1999) Modeling three-dimensional deformation in response to pumping of unconsolidated aquifers. Environ Eng Geosci 5(2):199–212

Comerlati A, Ferronato M, Gambolati G, Putti M, Teatini P (2004) Saving Venice by seawater. J Geophys Res 109, F03006. doi:10.1029/2004JF000119

COMSOL Multiphysics 5.0 (2014) COMSOL Inc. http://cn.comsol.com/subsurface-flow-module. Accessed February 2016

Ferronato M, Gambolati G, Teatini P (2001) Ill-conditioning of finite element poroelasticity equations. Int J Solids Struct 38(34–35):5995–6014

Ferronato M, Janna C, Pini G (2012) Parallel solution to ill-conditioned FE geomechanical problems. Int J Numer Anal Methods Geomech 36(4):422–437

Freeze RA, Cherry JA (1979) Groundwater. Prentice-Hall, Englewood Cliffs, NJ

Galloway DL, Burbey TJ (2011) Review: Regional land subsidence accompanying groundwater extraction. Hydrogeol J 19(8):1459–1486

Gambolati G, Freeze RA (1973) Mathematical simulation of the subsidence of Venice: 1, theory. Water Resour Res 9(3):721–733

Gambolati G, Teatini P, Baù D, Ferronato M (2000) The importance of poroelastic coupling in dynamically active aquifers of the Po River basin, Italy. Water Resour Res 36(9):2443–2459

Gambolati G, Ferronato M, Janna C (2011) Preconditioners in computational geomechanics: a survey. Int J Numer Anal Methods Geomech 35(9):980–996

Gu XY, Gong SL, Huang HC, Liu Y (1990) Quantitative study of land subsidence in Shanghai. Proc of the Sixth International Congress of IAEG, Amsterdam, August 1990, pp 1363–1370

Gu XY, Deng W, Xu DN, Liu Y (1993) Computation of land subsidence in Shanghai with secondary consolidation effect. Proc of the First International Conference on Soft Soil Engineering, Guangzhou, China, November 1993, pp 65–70

Helm DC (1994) Horizontal aquifer movement in a Theis-Thiem confined aquifer. Water Resour Res 30(4):953–964

Janna C, Ferronato M, Gambolati G (2010) A Block FSAI-ILU parallel preconditioner for symmetric positive definite linear systems. SIAM J Sci Comput 32:2468–2484

Li Q, Su H (1991) A study on three dimensional groundwater flow model in Shanghai. Shanghai Geol 39:28–37

Luo Y, Ye S, Wu J, et al (2016) A modified inverse procedure for calibrating parameters in land subsidence model and its field application in Shanghai, China. Hydrogeol J. doi:10.1007/s10040-016-1381-3

Shi X, Wu J, Ye S et al (2008) Regional land subsidence simulation in Su-Xi-Chang area and Shanghai City, China. Eng Geol 100:27–42

Teatini P, Ferronato M, Gambolati G, Gonella M (2006) Groundwater pumping and land subsidence in the Emilia-Romagna coastland, Italy: modeling the past occurrence and the future trend. Water Resour Res 42, W01406. doi:10.1029/2005WR004242

Teatini P, Ferronato M, Gambolati G, Baù D, Putti M (2010) Anthropogenic Venice uplift by seawater pumping into a heterogeneous aquifer system. Water Resour Res 46, W11547. doi:10.1029/2010WR009161

Teatini P, Castelletto N, Ferronato M, Gambolati G, Tosi L (2011) A new hydrogeologic model to predict anthropogenic uplift of Venice. Water Resour Res 47, W12507. doi:10.1029/2011WR010900

Verruijt A (1969) Elastic storage of aquifers. In: Wiest RJM (ed). Flow through porous media, Academic Press, New York, pp 331–376

Wang GY, You G, Shi B et al (2009) Earth fissures triggered by groundwater withdrawal and coupled by geological structures in Jiangsu Province, China. Environ Geol 57(5):1047–1054

Wu J, Shi X, Ye S et al (2010) Numerical simulation of viscoelastoplastic land subsidence due to groundwater overdrafting in Shanghai, China. J Hydrol Eng 15(3):223–236

Xue Y, Wu J, Zhang Y, Ye S et al (2008) Simulation of regional land subsidence in the southern Yangtze Delta. Sci China Ser D Earth Sci 51(6):808–825

Ye S (2004) Study on the regional land subsidence model and its application. PhD Thesis, Nanjing University, China

Ye S, Xue Y, Wu J, et al (2005) Study on the groundwater flow model for land subsidence modeling in Shanghai. Proc of the Seventh International Symposium on Land Subsidence, Shanghai, China, October 2005, pp 628–634

Ye S, Xue Y, Wu J et al (2011) Regional land subsidence model embodying complex deformation. P I Civil Eng-Wat M 164(WM10):519–531

Ye S, Xue Y, Wu J et al (2012) Modeling visco-elastic–plastic deformation of soil with Modified Merchant Model. Environ Earth Sci 66:1497–1504

Zhang AG, Wei ZX (2002) Past, present and future research on land subsidence in Shanghai (in Chinese). Hydrogeol Eng Geol 33(5):72–75